Johann Radon Institute for
Computational and Applied Mathematics
Austrian Academy of Sciences (ÖAW)

Tomographic Reconstruction for Single Conjugate Adaptive Optics

J. Niebsch, R. Ramlau

RICAM-Report 2021-25

Tomographic Reconstruction for Single Conjugate Adaptive Optics

Jenny Niebsch* Ronny Ramlau†‡

May 11, 2020

Abstract

Single Conjugate Adaptive Optic systems use the light of one bright guide star and a deformable mirror to correct for the loss of image quality of earthbound astronomical telescopes caused by turbulences in the atmosphere. The system achieves best correction in guide star direction. The imaging quality of the scientific object, which is usually seperated from the guide star, can further be improved if the turbulence distribution is known. We propose to use wavefront sensor measurements from the past to recover the turbulence in the atmosphere. Mathematically, a limited angle tomography problem has to be solved. We present a model for the related tomography equations and discuss solvability and uniquenss of the solutions. Based on our analysis we develop an algorithm for the inversion and obtain a first numerical reconstruction.

*Johann Radon Institute Linz, Altenbergerstraße 69, A-4040 Linz, Austria, (jenny.niebsch@ricam.oeaw.ac.at)

†Johannes Kepler University Linz, Institute of Industrial Mathematics, Altenbergerstraße 69, A-4040 Linz, Austria, (ronny.ramlau@jku.at)

‡Johann Radon Institute Linz, Altenbergerstraße 69, A-4040 Linz, Austria, Corresponding author.

1 Introduction

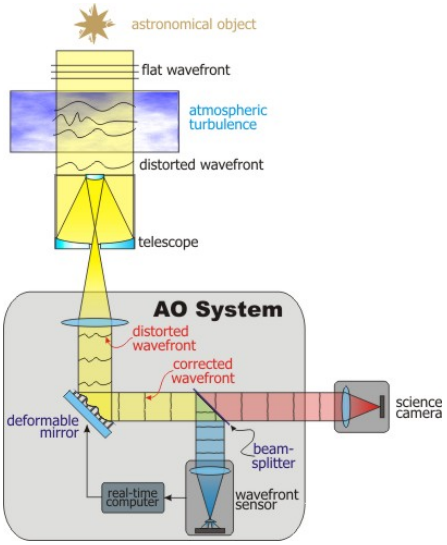

Figure 1: Sketch of SCAO system, taken from [4].

The image quality of modern earthbound astronomical telescopes suffers heavily from turbulences in the atmosphere. Patches of warm or cold air, located in layers of the atmosphere, distort the light coming from the scientific objects of interest, resulting in blurred images. This effect is in particular pronounced for the new generation of Extremely Large Telescopes (ELT) which are currently under construction. A remedy is the use of *Adaptive Optics (AO)*: These systems correct the aberrations of the incoming wavefronts of the scientific object by means of one or more deformable mirrors (DM). Based on measurements of the incoming wavefronts from one or several guide stars, the mirror shape is chosen such that the distortions from the incoming wavefront are corrected in the reflected wavefront. For a detailed description of the principles of Adaptive Optics we refer to [26, 27, 7].

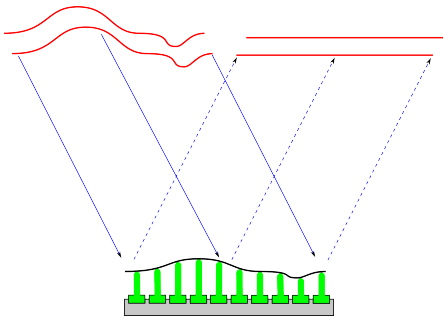

Figure 2: Correction of a wavefront by a deformable mirror [2].

There are different modes of operation for AO. The first - and simplest - is *Single Conjugate Adaptive Optics (SCAO)*, see Fig. 1. It is used if the scientific object is close

to a bright star that acts as a Natural Guide Star (NGS). As a point source that is far away, the incoming light from the NGS resembles a plane wave that is distorted by the turbulences in different layers of the atmosphere. A wavefront sensor (WFS) measures the incoming wavefront, and an Real Time Computing (RTC) system determines a shape of the DM that flattens the wavefront of the NGS, see Fig. 2, which is now recorded as a sharp image. As the light from the nearby scientific object passes through nearly the same part of the atmosphere the DM also corrects its image.
For objects that have no NGS nearby, tomography based AO systems are suitable. These systems use multiple guide stars - both natural and artificial - , each equipped with a wavefront sensor, and deformable mirrors for correction. Artificial guide stars are created by laser beams and therefore are called Laser Guide Stars (LGS). They are used whenever no suitable NGS is close by. Modern AO systems, e.g. for the ELT, will be equipped with up to 6 LGS. The incoming wavefronts from the different Guide Stars are used for a tomography of the atmosphere, i.e., the turbulence distribution of the atmosphere above the telescope is reconstructed. The underlying mathematical problem is a limited angle tomography and therefore severely ill-posed [3, 17]. However, as we only strive to reconstruct a layered atmosphere composed of a finite number of layers, the ill-posedness of the problem is somewhat mitigated, see [18]. Three different AO systems are based on atmospheric tomography: *Multi Conjugated Adaptive Optics (MCAO)*, *Laser Tomography (LTAO)* and *Multi Object Adaptive Object (MOAO)*. LTAO uses the reconstructed atmosphere and one DM which is deformed s.t. the scientific object of interest is optimally sharpened. MOAO is based on the same concept, but uses several mirrors that are optimized to sharpen separated objects at the same time. In contrast, MCAO uses up to three different mirrors, conjugated to different heights, to achieve a high imaging quality on a large connected patch of the sky, thus allowing to observe larger structures. See also Fig. 3 for the different systems. Let us finally remark that all computations required for the control of the DMs need to be done in real time, and have to be repeated about every 2ms for the full observation process. For further information on the systems we refer to [14, 1, 24, 20, 5] and for the mathematics of atmospheric tomography we refer to [8, 6, 10, 11, 33, 12, 9, 25, 32, 31, 23, 29, 22, 15, 34, 30, 21].

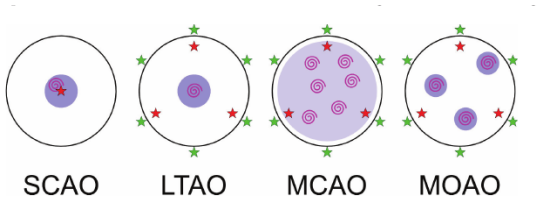

Figure 3: Different operating modes of AO systems. Light blue marks the area of corrected imaging quality [2].

As mentioned above, the imaging quality for a SCAO system decreases the further the scientific object is away from the Guide Star. A knowledge of the turbulence distribution of the atmospheric layers would therefore also be useful in the SCAO case, as it would allow for a better estimate of the wavefront aberration in the direction of the observed object. Of course, a tomography of the atmosphere based on measurements from one direction is impossible. Our idea of a tomography-like reconstruction of the atmosphere for SCAO is based on the fact that the layers are blown over the telescope

by a - at least on small time scales - constant wind velocity while the layers themself are not changing (frozen flow assumption, see, e.g., [27]). Please note that wind speed and direction might be different for each layer. Basically, the measurements from the wavefront sensor at different time steps are created by shifted turbulent layers. As we will see, the connection of the data for a certain number of time steps and the turbulence of the layers can be described by a system of equations that is very similar to the atmospheric tomography. We may add that frozen flow assumption has been used previously for a better estimate of the measured wavefront [19].

The paper is organized as follows: In Section 2.1 we give a short overview about wavefront reconstruction from sensor measurements in SCAO. In Section 2.2 the tomography operator for SCAO will be derived, whereas Section 2.3 focuses on solvability and uniqueness of the resulting operator equation. Section 2.4 decomposes the tomography operator on a rectangular domain using the Fourier basis of $Ł_2([-R,R]^2)$. Section 3 contains the description of the reconstruction algorithm, the test setting and numerical results of a simulation to test the feasibility of our approach. We close with a short summary and an outlook to future work.

2 A mathematical approach for Tomography for SCAO

In this section we will present the general idea of SCAO - Tomography as well as the related tomography equations. The Fourier representation of this operator on a rectangular domain allows to derive conditions for the (unique) solvability of the problem. As a consequence, conditions on the model of the atmosphere and the number of time steps used for the reconstruction can be derived.

2.1 Wavefront reconstruction for SCAO

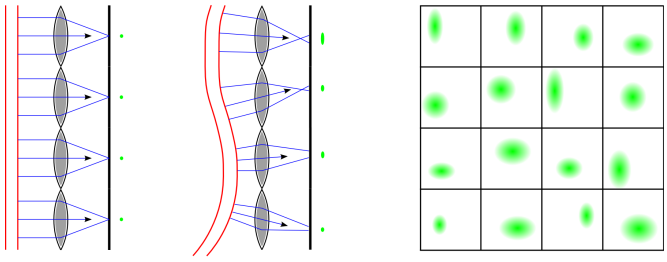

Figure 4: Sketch of a Shack-Hartmann Sensor with 16 subapertures. The deviation of the center of the recorded spots from the center of each subaperture Ω_i (in x and y direction are the measurements (s_x^i, s_y^i) [2].

As already mentioned in the introduction, SCAO is the simplest AO system, utilising one deformable mirror, optically conjugated to the ground layer of the atmosphere, and one wavefront sensor. The telescope is positioned such that the NGS is located in the centre of the field of view and the light emitted from the NGS approximately propagates in direction of the zenith to the telescope aperture. The WFS measures

the incoming wavefront of the NGS, i.e., it sees summed turbulence contributions of the layers in that direction. Based on the sensed incoming wavefront, the deformable mirror is adapted in such a way that it compensates for this wavefront. Unfortunately, the sensor cannot measure the wavefronts directly. E.g., a Shack-Hartmann sensor, Fig. 4, measures averaged gradients in x- and y-direction over sub-apertures of the sensor. Measurements $\mathbf{s}$ and the related WF φ are connected via the WFS operator Γ. For the Shack-Hartmann sensor, the WFS operator is given by

$$\mathbf{s} = (s_x^i, s_y^i)_{i\in I} = \Gamma\varphi, \tag{1}$$

$$s_x^i := \int_{\Omega_i} \frac{\partial}{\partial x}\varphi(x,y)\,dx, \tag{2}$$

$$s_y^i := \int_{\Omega_i} \frac{\partial}{\partial y}\varphi(x,y)\,dy. \tag{3}$$

The shape of the mirror can be derived directly from the wavefront. However, in order to dertermine the wavefront φ from wavefront measurements, equation (1) has to be solved about every $1-2$ ms due to the fast changing atmosphere. Several methods were developed to compute φ from the data $\mathbf{s}$. MVM methods connect the correction commands for the DM and the sensor data via a single control matrix which requires matrix-vector-multiplication (MVM) to solve the problem, leading to a numerical complexity of $\mathcal{O}(N^2)$. As the number of measurements grows with the size of the telescopes, faster algorithms have been developed to guarantee real time reconstruction. A matrix free approach for the reconstruction of wavefronts from sensor data in real time is the CuReD algorithm (Cumulated Reconstructor with Domain decomposition), [35, 28].

Our approach is based on the wavefronts instead of the measurements, thus we assume that the wavefronts have already been reconstructed by a suitable reconstruction method.

2.2 Derivation of the tomography equations

In classical SCAO as described in Section 2.1, the best correction is in direction of the NGS. The quality of the image of the observed scientific object decreases rapidly with increasing angular distance from the NGS, as the WF emitted by that object takes a different path through the atmosphere than the NGS and therefore is not optimally compensated by the DM. Incorporating a reconstruction of the atmosphere in the SCAO mode would enable us to correct the incoming WF from the scientific object. The observation quality, i.e., the Strehl ratio (which is closely related to the L_2 error of the reconstruction) of the object is expected to improve while the Strehl ratio in direction of the NGS will probably decrease.

In modelling the effect of the turbulence we will use the assumption that the atmosphere has a layered structure, and that the effect of the layered turbulence distribution on a planar wavefront can be expressed by the summation of the turbulent layers in the appropriate directions, see, e.g., [8]. More specific, the incoming wavefront $\varphi(\mathbf{r},t)$ at the telescope aperture Ω_A can be written as the sum of the turbulence contributions of

the layer functions $\Phi^{(l)}$, i.e.,

$$\varphi(\mathbf{r},t) = \sum_{l=1}^{L} \Phi^{(l)}(\mathbf{r},t), \tag{4}$$

where $\boldsymbol{r} \in \Omega_A$ represents the 2D spatial coordinates in the telescope pupil and t indicates the time. Based on the Taylor frozen flow assumption, which states that each layer propagates with its own speed and direction, represented by the wind shift vector $\mathbf{v}_l \in \mathbb{R}^2$, the temporal evolution of the single layers from time $t-\tau$ to t can be attributed to a spatial shift with displacement $\tau\mathbf{v}_l$, i.e.,

$$\Phi^{(l)}(\mathbf{r}, t-\tau) = \Phi^{(l)}(\mathbf{r} + \tau\mathbf{v}_l, t). \tag{5}$$

Assuming equidistant time steps Δ_T and choosing $\tau = k\Delta_T$ we have

$$\Phi^{(l)}(\mathbf{r}, t-k\Delta_T) = \Phi^{(l)}(\mathbf{r} + k\Delta_T\mathbf{v}_l, t), \tag{6}$$

see also [19]. We can use (6) to compute the layers $\Phi^{(l)}$ at the actual time t from data of the previous time steps $(t-k\Delta_T), k = 0, \cdots, K$. Using (4), (6), the incoming wavefronts at different time steps can be computed as

$$\varphi_k := \varphi(\mathbf{r}, t-k\Delta_T) = \sum_{l=1}^{L} \Phi^{(l)}(\mathbf{r} + k\Delta_T\mathbf{v}_l, t), \tag{7}$$

see Fig. 5 for an illustration.

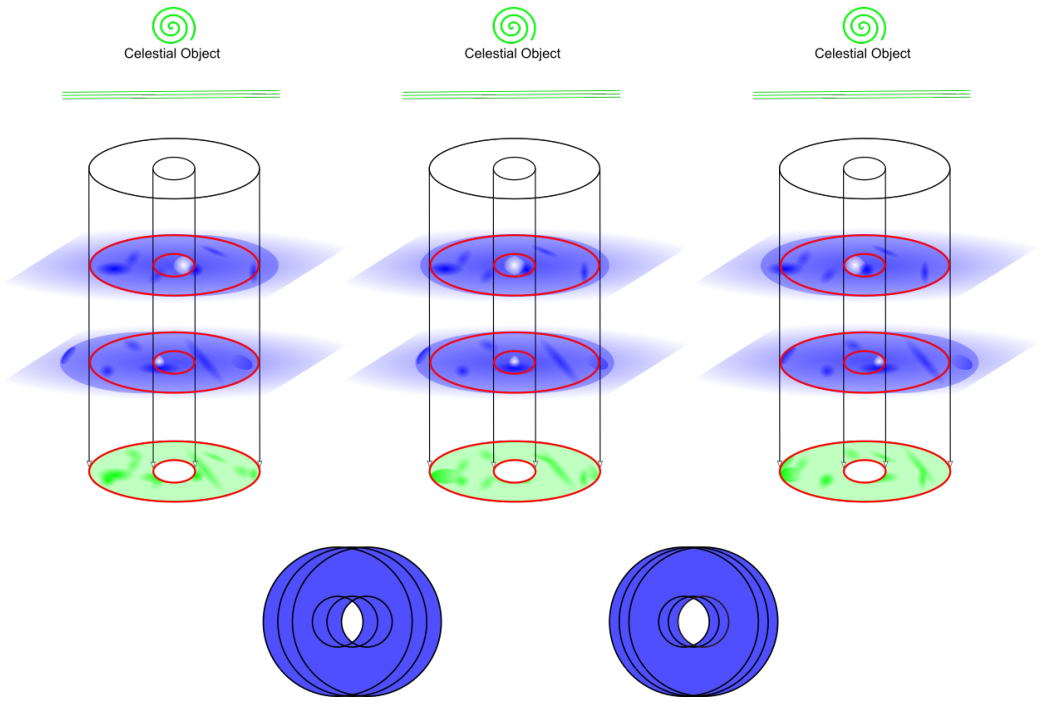

Figure 5: Illustration of the the turbulence contributions of the layers $\Phi^{(1)}$ and $\Phi^{(2)}$ to the incoming wavefronts $\varphi_3, \varphi_2, \varphi_1$. The telescope aperture is restricted by the red circles. The dark blue areas on the turbulent layers belongs to those atmospheric cutouts which contribute to the incoming wavefronts of the evolution equations. The picture below shows the support of the layer functions.

Please note that we assume that the wind vectors $\mathbf{v}_l$ are explicitly known. We wish, however, to remark that techniques are available to either estimate the wind vectors from the wavefront sensor measurements or to measure them directly with an additional instrument [19].

Equation (7) forms the basis for our tomography equation. We define by $\Omega_A(k\Delta_T\mathbf{v}_l) = \{\mathbf{r} \in \mathbb{R}^2 : \mathbf{r} - k\Delta_T\mathbf{v}_l \in \Omega_A\}$ the area of layer l seen by the telescope at time step k and $\Omega_l = \bigcup_{k=0}^{K} \Omega_A(k\Delta_T\mathbf{v}_l)$. Since we also want to consider the Fourier transform of the tomography equation we define the rectangular area $\bar{\Omega} = [-R, R]^2$ where R is the smallest number such that $\bigcup_{l=1}^{L} \Omega_l \subset [-R, R]^2$.

Setting $X = L^2(\bar{\Omega})$, and, for a fixed time t, $\Phi^{(l)}(\mathbf{r}, t) = \Phi^{(l)}(\mathbf{r}) \in X$ for $l = 1, \cdots, L$, we define the operator $\mathbf{A}_k : \prod_{l=1}^{L} X \to X$ as

$$(\mathbf{A}_k\mathbf{\Phi})(\mathbf{r}) \quad := \quad \sum_{l=1}^{L} \Phi^{(l)}(\mathbf{r} + \mathbf{v}_l k\Delta_T), \qquad \mathbf{r} \in \bar{\Omega}, \tag{8}$$

where $\mathbf{\Phi} = (\Phi^{(1)}, \cdots, \Phi^{(L)})$ represents the full layered atmosphere. With definition (8) and (7) the tomography-like operator equation at time t is then given as

$$\mathbf{A}\mathbf{\Phi} \quad := \quad \begin{pmatrix} \mathbf{A}_0\mathbf{\Phi} \\ \mathbf{A}_1\mathbf{\Phi} \\ \vdots \\ \mathbf{A}_K\mathbf{\Phi} \end{pmatrix} = \begin{pmatrix} \varphi_0 \\ \varphi_1 \\ \vdots \\ \varphi_K \end{pmatrix} =: \boldsymbol{\varphi}, \tag{9}$$

$$\text{with} \quad \mathbf{A} \quad : \quad \prod_{l=1}^{L} X \to \prod_{j=1}^{K+1} X.$$

Now the computation of the turbulence profile reduces to the solution of eq. (9).

2.3 Solvability and uniqueness

In this section we focus on the existence of solutions of our tomography equation as well as on the uniqueness. As a shift in a function is nicely represented by the Fourier transform, the shift in the layers in (8) suggests to consider the tomography equation in the Fourier space in order to derive necessary conditions for the solvability and uniqueness of the tomography equation (9).

In the following, we use the 2-D Fourier transform on $\mathbb{R}^2$ defined as

$$(\mathcal{F}f)(\mathbf{s}) = \int_{\mathbb{R}^2} f(\mathbf{r}) e^{-2\pi i \langle \mathbf{r}, \mathbf{s} \rangle} d\mathbf{r},$$

where $\langle \cdot, \cdot \rangle$ is the usual inner product on $\mathbb{R}^2$.

For our theoretical analysis we assume that the atmosphere layer functions and the wavefronts are defined on $\mathbb{R}^2$. Specifically, we require that

Assumption 1 *For the layers* $\mathbf{\Phi} = \left(\Phi^{(1)}, \dots, \Phi^{(L)}\right)$ *holds* $\Phi^{(l)} \in L^1(\mathbb{R}^2) \cap L^2(\mathbb{R}^2)$.

Remark 1 *Turbulences in the atmosphere can be modelled either by a Kolmogrov or a van Karman statistics [27]. Thus, in average, the turbulent layers belong to the Sobolev space* $H^{11/6}(\mathbb{R}^2)$ *and thus also to* $L^2(\mathbb{R}^2)$. *As there is anyway no hope to reconstruct the atmosphere outside the area where there are measurements available, we can extend the layers outside this area by zero or simply assume that the layers are compactly supported. In this case the layer will also belong to* $L^1(\mathbb{R}^2)$.

Equation (9) in the Fourier domain is given by

$$(\mathcal{F}\mathbf{A}\mathbf{\Phi})(\mathbf{s}) = \begin{pmatrix} (\mathcal{F}\mathbf{A}_0\mathbf{\Phi})(\mathbf{s}) \\ (\mathcal{F}\mathbf{A}_1\mathbf{\Phi})(\mathbf{s}) \\ \vdots \\ (\mathcal{F}\mathbf{A}_K\mathbf{\Phi})(\mathbf{s}) \end{pmatrix} = \begin{pmatrix} (\mathcal{F}\varphi_0)(\mathbf{s}) \\ (\mathcal{F}\varphi_1)(\mathbf{s}) \\ \vdots \\ (\mathcal{F}\varphi_K)(\mathbf{s}) \end{pmatrix},$$

where the Fourier transform is applied componentwise. Because of the linearity and the time shifting property of the Fourier transform,

$$(\mathcal{F}f(\mathbf{r} - \mathbf{r}_0))(\mathbf{s}) = e^{-2\pi i\langle \mathbf{r}_0, \mathbf{s}\rangle}(\mathcal{F}f(\mathbf{r}))(\mathbf{s}),$$

we have for each $k = 0, \cdots, K$,

$$(\mathcal{F}\mathbf{A}_k\mathbf{\Phi})(\mathbf{s}) = \sum_{l=1}^{L} e^{2\pi i\langle \mathbf{v}_l k\Delta_T, \mathbf{s}\rangle}(\mathcal{F}\Phi^{(l)}(\mathbf{r}))(\mathbf{s}) = (\mathcal{F}\varphi_k)(\mathbf{s}).$$

Hence the Fourier transform of (9) can be expressed in matrix form as

$$\begin{pmatrix} (\mathcal{F}\varphi_0)(\mathbf{s}) \\ (\mathcal{F}\varphi_1)(\mathbf{s}) \\ \vdots \\ (\mathcal{F}\varphi_K)(\mathbf{s}) \end{pmatrix} = \underbrace{\begin{pmatrix} 1 & \cdots & 1 \\ e^{\Delta_T 2\pi i\langle \mathbf{v}_1, \mathbf{s}\rangle} & \dots & e^{\Delta_T 2\pi i\langle \mathbf{v}_L, \mathbf{s}\rangle} \\ \vdots & \ddots & \vdots \\ e^{K\Delta_T 2\pi i\langle \mathbf{v}_1, \mathbf{s}\rangle} & \dots & e^{K\Delta_T 2\pi i\langle \mathbf{v}_L, \mathbf{s}\rangle} \end{pmatrix}}_{=:\mathbf{F}(\mathbf{s})} \begin{pmatrix} (\mathcal{F}\Phi^{(1)})(\mathbf{s}) \\ (\mathcal{F}\Phi^{(2)})(\mathbf{s}) \\ \vdots \\ (\mathcal{F}\Phi^{(L)})(\mathbf{s}) \end{pmatrix}. \quad (10)$$

Representation (10) allows to link the solvability of the tomography eqation to the invertibility of the matrix $\mathbf{F}(\mathbf{s})$.

Proposition 1 *Assume that for* $l, m = 1, \cdots, L$ *and* $l \neq m$ *holds* $\mathbf{v}_l \neq \mathbf{v}_m$.

(1) The matrix $\mathbf{F}(\mathbf{0})$ *has rank 1.*

(2) Assume that for $\mathbf{s} \neq \mathbf{0}$ *holds for all* $n \in \mathbb{Z}$

$$\langle \mathbf{v}_l - \mathbf{v}_m, \mathbf{s}\rangle \neq \frac{n}{\Delta_T}. \quad (11)$$

Then the columns of $\mathbf{F}(\mathbf{s})$ *in (10) are linearly independent if* $L \leqslant K + 1$ *and linearly dependent if* $L > K + 1$.

Proof. (1) If $\mathbf{s} = \mathbf{0}$, then all entries in $\mathbf{F}(\mathbf{0})$ are equal to 1, and therefore $\mathbf{F}(\mathbf{0})$ has rank 1.
(2) Let $x_l := e^{\Delta_T 2\pi i \langle \mathbf{v}_l, \mathbf{s}\rangle}$, $l = 1, \cdots, L$. Because of (28), $x_l \neq x_m$ holds for all $l \neq m$, $l, m = 1, \cdots, L$. With $e^{k\Delta_T 2\pi i \langle \mathbf{v}_l, \mathbf{s}\rangle} =: x_l^k$ for $k = 1, \cdots, K$, the matrix $\mathbf{F}(\mathbf{s})$ is a Vandermonde matrix

$$\mathbf{F} = \begin{pmatrix} 1 & \cdots & 1 \\ x_1 & \cdots & x_L \\ x_1^2 & \cdots & x_L^2 \\ \vdots & \ddots & \vdots \\ x_1^K & \cdots & x_L^K \end{pmatrix}. \tag{12}$$

In case $L = K + 1$, its determinant can be computed as $\prod_{l=2}^{L} \prod_{m=1}^{l-1} (x_l - x_m)$, [16], and it is nonzero under our assumptions and therefore $\mathbf{F}$ has linearly independent columns.
In case $L < K + 1$, the matrix (12) can be expanded with $N = K + 1 - L$ columns $(1, x_{L+j}, x_{L+j}^2, \cdots, x_{L+j}^K)^T$ for $j = 1, \cdots, N$, where the x_{L+j} are chosen distinct from all x_l and from each other. The expanded matrix is a square Vandermonde matrix hence all columns are linearly independent which implies that the first L columns are as well.
In case $L > K + 1$, the first $K + 1$ columns are linearly independent with the same argument as in above and form a basis of $\mathbb{C}^{K+1}$. It follows that the remaining column vectors are linearly dependent on the first $K + 1$ column vectors. □

Whenever $\mathbf{v}_l \neq \mathbf{v}_m$ and condition (28) hold, then $\mathbf{F}(\mathbf{s})$ is invertible, and thus the Fourier transform of the turbulent layers is uniquely reconstructable for those $\mathbf{s}$. For the remaining $\boldsymbol{s}$ we have the following result:

Proposition 2 *Assume that for $l, m = 1, \cdots, L$ and $l \neq m$ holds $\mathbf{v}_l \neq \mathbf{v}_m$. Further, assume that either $\mathbf{s} = 0$ or*

$$\langle \mathbf{v}_l - \mathbf{v}_m, \mathbf{s}\rangle = \frac{n}{\Delta_T}. \tag{13}$$

holds for some $l \neq m$, $l, m = 1, \ldots, L$, $n \in \mathbb{Z}$ and $\mathbf{s} \neq \mathbf{0}$. Then there exists a sequence $\mathbf{s}_k \to \mathbf{s}$ as $k \to \infty$, and $\mathbf{F}(\mathbf{s}_k)$ is invertible.

Proof. We start with the case $\boldsymbol{s} \neq \mathbf{0}$. If (13) holds for some (l, m) and $n \neq 0$, we set $\mathbf{s}_k := (1 - \frac{1}{k})\mathbf{s} \neq 0$ for $k \in \mathbb{N}$ and $k > 1$. Clearly, $\mathbf{s}_k \to \mathbf{s}$ as $k \to \infty$, and

$$\langle \mathbf{v}_l - \mathbf{v}_m, \mathbf{s}_k\rangle = (1 - \frac{1}{k})\frac{n}{\Delta_T} \to \frac{n}{\Delta_T}.$$

As of course also $\langle \mathbf{v}_l - \mathbf{v}_m, \mathbf{s}_k\rangle \neq \frac{n}{\Delta_T}$, $\mathbf{F}(\mathbf{s}_k)$ is invertible at least for large k.
Now assume that

$$\langle \mathbf{v}_l - \mathbf{v}_m, \mathbf{s}\rangle = 0$$

for some (l, m). We set $\mathbf{s}_k := (1 - \frac{1}{k})\boldsymbol{s} + \frac{1}{k}(\mathbf{v}_l - \boldsymbol{v}_m)$ and obtain

$$\begin{aligned} \langle \mathbf{v}_{\tilde{l}} - \mathbf{v}_{\tilde{m}}, \mathbf{s}_k\rangle &= \langle \mathbf{v}_{\tilde{l}} - \mathbf{v}_{\tilde{m}}, \mathbf{s}\rangle + \frac{1}{k}\langle \mathbf{v}_{\tilde{l}} - \mathbf{v}_{\tilde{m}}, \mathbf{v}_l - \mathbf{v}_m\rangle & (14) \\ &= \begin{cases} \frac{c_{\tilde{l},\tilde{m}}}{k}\|\mathbf{v}_l - \mathbf{v}_m\|^2 \text{ if } (\mathbf{v}_l - \mathbf{v}_m) \parallel (\mathbf{v}_{\tilde{l}} - \mathbf{v}_{\tilde{m}}) \\ (1 - \frac{1}{k})\langle \mathbf{v}_{\tilde{l}} - \mathbf{v}_{\tilde{m}}, \mathbf{s}\rangle + \frac{1}{k}\langle \mathbf{v}_{\tilde{l}} - \mathbf{v}_{\tilde{m}}, \mathbf{v}_l - \mathbf{v}_m\rangle \end{cases} & (15) \\ &\neq \frac{n}{\Delta_T}, & (16) \end{aligned}$$

$n \in \mathbb{Z}$, at least for a subsequence of a $\mathbf{s_k}$, and thus $\mathbf{F}$ is invertible on the subsequence. Please note that the above argument only holds as the wind vectors are elements in $\mathbb{R}^2$. It remains to consider the case $\mathbf{s} = \mathbf{0}$. Now we choose a vector $\mathbf{v} \in \mathbb{R}^2$ such that $\langle \mathbf{v}_l - \mathbf{v}_m, \mathbf{v} \rangle \neq 0$ for all (l, m) and set $\mathbf{s}_k := \frac{1}{k} v$. It follows again that there exists at least a subsequence of $\mathbf{s}_k$ such that

$$\langle \mathbf{v}_l - \mathbf{v}_m, \mathbf{s}_k \rangle \neq \frac{n}{\Delta_T},$$

and $\mathbf{F}(\mathbf{s}_k)$ is again invertible, which concludes the proof. □

Now we are able to give a result on the unique solvability.

Proposition 3 *Assume that $\Phi^{(l)} \in L^1(\mathbb{R}^2) \cap L^2(\mathbb{R}^2)$, $l = 1, \ldots, L$ and that the wind speed vectors $\mathbf{v}_l$ fulfill the condition $\mathbf{v}_l - \mathbf{v}_m \neq 0$ for $m \neq l$ and $l, m = 1, \ldots, L$. Then $\mathbf{\Phi} = (\Phi^{(1)}, \ldots, \Phi^{(L)})$ is uniquely reconstructable if $L \leqslant K + 1$.*

Proof. If $L \leqslant K + 1$ then $\mathbf{F}(\mathbf{s})$ is invertible as long as (28) holds. According to (10), $\mathcal{F}\left(\Phi^{(l)}\right)$ is thus well defined by the measurements. Now assume (28) is violated, i.e., (13) holds. According to Proposition 2 for those $\mathbf{s}$ there exists a sequence $\mathbf{s}_k \to \mathbf{s}$ where $\mathbf{F}(\mathbf{s_k})$ is invertible and therefore the related values of $\mathcal{F}\left(\Phi^{(l)}\right)(\mathbf{s}_k)$ are uniquely defined by the measurements. As $\Phi^{(l)} \in L^1$, its Fourier transform $\mathcal{F}\left(\Phi^{(l)}\right)$ is continuous and therefore $\mathcal{F}\left(\Phi^{(l)}\right)(s) := \lim_{k\to\infty} \mathcal{F}\left(\Phi^{(l)}\right)(\mathbf{s}_k)$ is uniquely determined. □

From Proposition 1 it follows that the assumption that the wind shifts of the layers are distinct is vital. It is also quite natural: Assume that we are given an atmosphere composed of two layers that move with the same speed and in the same direction. It follows immediately from (8) that the wavefronts φ_k at time step $k\Delta_T$ is just the shifted version of φ_0 and thus contains no additional information of the layered atmosphere. More general, all layers that move with the same wind vector behave in the data like a single layer that contains the sum of the turbulence contributions from those layers and can therefore not be reconstructed uniquely.
The matrix $\mathbf{F}$ is invertible if the number of time steps K is chosen as $L-1$, i.e., including the data from time frame i the number of data equals the number of layers. If the wind shifts are not distinct or if $L > K + 1$, then a least squares solution can be obtained by applying the generalized inverse $\mathbf{F}^\dagger = (\mathbf{F}^*\mathbf{F})^{-1}\mathbf{F}^*$ [13]. This is summarised in

Corollary 1 *Under the assumptions of Proposition 1 the solution of the tomography equation on $L^2(\mathbb{R}^2)$ is given by*

1. $$\mathbf{\Phi}(\mathbf{r}) = \mathcal{F}^{-1}(\mathbf{F}^{-1}(\mathbf{s})(\mathcal{F}\boldsymbol{\varphi})(\mathbf{s}))(\mathbf{r}), \quad \textit{if} \quad K = L - 1,$$

2. $$\begin{aligned} \mathbf{\Phi}(\mathbf{r}) &= \mathcal{F}^{-1}(\mathbf{F}^{+}(\mathbf{s})(\mathcal{F}\boldsymbol{\varphi})(\mathbf{s}))(\mathbf{r}) \quad \textit{otherwise} \\ \textit{with} \quad \mathbf{F}^\dagger &= (\mathbf{F}^*\mathbf{F})^{-1}\mathbf{F}^*. \end{aligned}$$

Assuming a certain number of layers in the atmosphere, the time steps taken into consideration must be at least of the same number or more. This is confirmed by numerical test computations. The assumption that the wind shift vectors of the layers are not equal (although they can be parallel) is reasonable. In case the vector $(\langle \mathbf{v}_1, \mathbf{s}\rangle, \cdots, \langle \mathbf{v}_L, \mathbf{s}\rangle)$ is zero or close to it the matrix $\mathbf{F}$ is rank deficient.

2.4 A Fourier series representation of the tomography operator

In a real life situation wavefronts can only be determined on the telescope aperture. In a first approximation of the real data situation we assume that the layer functions as well as the wavefronts are defined on $\bar{\Omega} = [-R, R]^2$. As in (9), it makes now sense to use the Fourier series representation of the layer and wavefront functions instead of the Fourier transform on $\mathbb{R}^2$. We assume that the functions in $L^2(\bar{\Omega})$ are complex (complex unit i) valued and define an orthonormal basis of $L^2(\bar{\Omega})$ by

$$\omega_{jm}(x, y) := \frac{1}{2R} e^{i\frac{\pi}{R}(jx+my)}, \qquad j, m \in \mathbb{Z}. \tag{17}$$

Next, we decompose the projection operators $\mathbf{A}_k$ in (8) with respect to this basis. Each $\Phi^{(l)}(x, y) \in L^2(\bar{\Omega}),\ l = 1, \cdots, L$, has the representation

$$\begin{aligned} \Phi^{(l)}(x, y) &= \sum_{j,m\in\mathbb{Z}} \Phi^{(l)}_{jm}\, \omega_{jm}(x, y) \qquad \text{with} \\ \Phi^{(l)}_{jm} &= \langle \Phi^{(l)}, \omega_{jm}\rangle_{L^2(\bar{\Omega})}. \end{aligned}$$

With the notation

$$\mathbf{\Phi}_{jm} = (\Phi^{(1)}_{jm}, \cdots, \Phi^{(L)}_{jm})^T,$$

we can represent the full atmosphere as

$$\mathbf{\Phi} = \sum_{j,m\in\mathbb{Z}} \mathbf{\Phi}_{jm}\, \omega_{jm}, \tag{18}$$

where the summation of a vector has to be understood componentwise. Now (8) can be written as

$$\begin{aligned} (\mathbf{A}\mathbf{\Phi})_k(x, y) &= \sum_{l=1}^{L} \sum_{j,m\in\mathbb{Z}} \Phi^{(l)}_{jm}\, \omega_{jm}(x + v^{(l)}_x k\Delta_T, y + v^{(l)}_y k\Delta_T) \\ &= \sum_{j,m\in\mathbb{Z}} \left(\sum_{l=1}^{L} \Phi^{(l)}_{jm}\, \underbrace{2R \cdot \omega_{jm}(j\ v^{(l)}_x k\Delta_T, m\ v^{(l)}_y k\Delta_T)}_{=:(A_{jm})_{k,l}} \right) \omega_{jm}(x, y). \end{aligned}$$

Denoting by $\varphi^k_{jm},\ k = 0, \cdots, K$, the Fourier coefficients of φ_k and by

$$\boldsymbol{\varphi}_{jm} = (\varphi^0_{jm}, \cdots, \varphi^K_{jm})^T), \tag{19}$$

we have

$$(\mathbf{A}\mathbf{\Phi})(x, y) = \sum_{j,m\in\mathbb{Z}} (A_{jm}\mathbf{\Phi}_{jm})\, \omega_{jm}(x, y) = \sum_{j,m\in\mathbb{Z}} \boldsymbol{\varphi}_{jm}\, \omega_{jm}(x, y), \tag{20}$$

and therefore the Fourier coefficients $\boldsymbol{\varphi}_{jm}$ of the wavefront can be computed from the Fourier coefficients of the atmosphere layers $\boldsymbol{\Phi}_{jm}$ for each j and m by

$$\boldsymbol{\varphi}_{jm} = A_{jm}\boldsymbol{\Phi}_{jm}, \tag{21}$$

i.e., the compution of the wavefronts (and therefore also the inverse operation) *decouples* for each (j, m). This is also reflected in

Proposition 4 *Let A_{jm}, $\boldsymbol{\varphi}_{jm}$ and $\boldsymbol{\Phi}_{jm}$ be defined as above. Then operator $\boldsymbol{A}$ can be described in terms of its action on the Fourier coefficients of the turbulent layers and the wavefronts as*

$$\begin{pmatrix} \vdots \\ \boldsymbol{\varphi}_{jm} \\ \vdots \end{pmatrix} = diag(A_{jm}) \begin{pmatrix} \vdots \\ \boldsymbol{\Phi}_{jm} \\ \vdots \end{pmatrix} \tag{22}$$

where $diag(A_{jm})$ denotes a block diagonal matrix with the matrices A_{jm} on the diagonal and zeros outside.

Proof. Follows directly from (21). □

Please note that we are now in a similiar situation as in [18], where the authors consider a singular value decomposition of the standard atmospheric tomography operator. Specifically, the operator $\boldsymbol{A}$ relates directly to the matrix $diag(A_{jm})$ and

$$\begin{aligned} \boldsymbol{\varphi}_{jm} \in \mathbb{R}^K &\quad\leftrightarrow\quad \boldsymbol{\varphi}_{jm} \cdot \omega_{jm}(x, y) \in L_2(\bar{\Omega})^K \\ \boldsymbol{\Phi}_{jm} \in \mathbb{R}^L &\quad\leftrightarrow\quad \boldsymbol{\Phi}_{jm} \cdot \omega_{jm}(x, y) \in L_2(\bar{\Omega})^L. \end{aligned}$$

For each of the matrices A_{jm} there exists a singular system, i.e., vectors $v_{jm,n} \in \mathbb{C}^L, u_{jm,n} \in \mathbb{C}^K$, and numbers $\sigma_{jm,n}, n = 1, \ldots, r_{jm} \leqslant min\{L, K\}$ that satisfy

$$\begin{aligned} A_{jm}\boldsymbol{\Phi}_{jm} &= \sum_{n=1}^{r_{jm}} \sigma_{jm,n}\langle v_{jm,n}, \boldsymbol{\Phi}_{jm}\rangle u_{jm,n} \\ \langle v_{jm,l}, v_{jm,n}\rangle &= \delta_{ln}, \qquad \langle u_{jm,l}, u_{jm,n}\rangle = \delta_{ln} \\ \sigma_{jm,1} &\geqslant \ldots \geqslant \sigma_{jm,r_{jm}} > 0. \end{aligned} \tag{23}$$

Here, r_{jm} is the rank of the matrix A_{jm} and the $\sigma^2_{jm,n}$ are the positive eigenvalues of the matrices $A^H_{jm}A_{jm}$ and $A_{jm}A^H_{jm}$, respectively. We obtain

Proposition 5 *The operator $\boldsymbol{A}$ admits a singular value type decomposition*

$$\boldsymbol{A\Phi} = \sum_{j,m\in\mathbb{Z}} \left(\sum_{n=1}^{r_{jm}} \sigma_{jm,n}\langle v_{jm,n}, \boldsymbol{\Phi}_{jm}\rangle u_{jm,n} \right) \omega_{jm} \tag{24}$$

and the sequence $\{\sigma_{jm,n} : j, m \in \mathbb{Z}, n = 1, \ldots, r_{jm}\}$ are the singular values of $\boldsymbol{A}$. Further on,

$$\boldsymbol{A}^\dagger \boldsymbol{\varphi} = \sum_{j,m\in\mathbb{Z}} \left(\sum_{n=1}^{r_{jm}} \frac{\langle u_{jm,n}, \boldsymbol{\varphi}_{jm} \rangle}{\sigma_{jm,n}} v_{jm,n} \right) \omega_{jm} \tag{25}$$

and

$$\mathcal{N}(\boldsymbol{A})^\perp = span\{v_{jm,n} \cdot \omega_{jm} \,|\, j,m \in \mathbb{Z},\, 1 \leqslant n \leqslant r_{jk}\}. \tag{26}$$

If the vectors $\hat{v}_{jm,n} \in \mathbb{C}^L$, $1 \leqslant n \leqslant L - r_{jk}$, *are a basis of* $\mathcal{N}(A_{jm})$, *then the nullspace of* $\boldsymbol{A}$ *is given as*

$$\mathcal{N}(\boldsymbol{A}) = span\{\hat{v}_{jm,n}\omega_{jm} \,|\, j,m \in \mathbb{Z},\, 1 \leqslant n \leqslant L - r_{jk}\}. \tag{27}$$

For a proof we refer to [18], pp. 844.

Proposition 5 links the nullspace of the operator $\boldsymbol{A}$ to the nullspaces of the matrices A_{jm}. Specifically, each rank deficient matrix A_{jm} contributes to the nullspace of $\boldsymbol{A}$. Please note that the matrices A_{jm} are closely related to the matrices $\boldsymbol{F}(\boldsymbol{s})$ defined in (10). Specifically, replacing in $\boldsymbol{F}(\boldsymbol{s})$ in each matrix element $\boldsymbol{s}$ by (j,m) and 2π by $\frac{\pi}{R}$ gives the matrix A_{jm}. In particular, A_{jm} also is a Vandermonde matrix, and Proposition 1 holds accordingly for A_{jm} if $\boldsymbol{s}$ is replaced by (j,m) and the right hand side of (28) is replaced by $n \cdot \frac{2R}{\Delta T}$. Additionally, (28) immediately yields that **all** matrices A_{jm} are rank deficient if $\boldsymbol{v}_l = \boldsymbol{v}_m$ for some $m \neq l$, i.e., if at least two of the layers move with the same speed and direction. We also conclude from Proposition 1 that the matrix A_{00} has always rank 1, i.e., constant functions on the layers cannot be reconstructed. Figure 7, plotting the rank of the A_{jm}, shows that $\boldsymbol{A}$ has a nontrivial nullspace in the considered setting. In such a case, it is only possible to reconstruct the atmosphere in a least squares sense. Please note that this is not in contradiction to Proposition 3, as we are now in a periodic setting. We summarize these results in

Proposition 6 *Assume that for* $l,m = 1,\cdots,L$ *and* $l \neq m$ *holds* $\mathbf{v}_l \neq \mathbf{v}_m$.

(1) The matrix A_{00} *has rank 1.*

(2) Assume that for $(j,m) \neq (0,0)$ *holds for all* $n \in \mathbb{Z}$

$$\langle \mathbf{v}_l - \mathbf{v}_m, (j,m) \rangle \neq n \cdot \frac{2R}{\Delta_T}. \tag{28}$$

Then the columns of A_{jm} *are linearly independent if* $L \leqslant K+1$ *and linearly dependent if* $L > K+1$.

If $\mathbf{v}_l = \mathbf{v}_m$ *holds for some* $l \neq m$, *then all matrices* A_{jm} *are rank deficient.*

3 Numerical realization

3.1 Algorithm

In this paper we are only concerned with the reconstruction of the atmosphere, and neglect the reconstruction of the wavefronts from sensor data as well as the computation

of the commands for the deformable mirrors.
We assume therefore that the wavefronts φ_k for times $t_0, t_0 - 1\Delta_T, t_0 - 2\Delta_T, \cdots, t_0 - K\Delta_T$ are given. The reconstruction algorithm is based on the Fourier coefficients φ^k_{jm} of the wavefront (19) and its shifted versions, solving the subsystems (21) and computing the atmosphere via (18). We recall the definition of the matrices $A_{jm} \in \mathbb{R}^{K+1,L}$ as

$$(A_{jm})_{k,l} := 2R \cdot \omega_{jm}(j\ v_x^{(l)} k\Delta_T, m\ v_y^{(l)} k\Delta_T) \tag{29}$$

Clearly, the (A_{jm}) can be computed in advance for each $j, m \in \{-N_0, \cdots, N_0 - 1\}$ where N_0 is a cut-off index for the Fourier series. As mentioned above, the reconstruction process reduces to the solution of a sequence of small matrix vector systems, which can be done effciently with standard solvers. For our numerical tests, we used either the generalized inverse of A_{jm} or the conjugate gradient method to compute a solution of each equation (21). Please note that whenever a matrix A_{jm} is rank deficient, there is no hope to recover the original solution. Instead, we compute a least squares solution.

Algorithm 1 Reconstruction algorithm for the atmosphere $\mathbf{\Phi}$ at time t_0

Choose cut-off index N_0
Precompute A_{jm} for $j, m \in \{-N_0, \cdots, N_0 - 1\}$
Compute φ^k_{jm} and cut off according to $j, m \in \{-N_0, \cdots, N_0 - 1\}$
for $j, m = -N_0 \ldots N_0 - 1$ **do**
  $\mathbf{\Phi}_{jm} = \mathbf{solve}(A_{j,m}, \varphi_{jm})$
end for
Compute $\mathbf{\Phi} = \sum_{j,m=-N_0}^{N_0} \mathbf{\Phi}_{jm}\ \omega_{jm}$.

3.2 Test setting

For our test computations we used the in-house developed software package *MOST* to create an atmosphere, which produces a realistic atmosphere using a viable C_n^2 profile modeling the strength of turbulence. For a first reconstruction, we use a 3-layers atmosphere, see Table 1 for specifications. The telescope models the ELT of the European Southern Observatory with radius $R = 21m$, whereas the atmosphere is created on the square $[-23.5; 23.5]^2$.

	height	speed	direction (x, y)	C_n^2-profile
1.layer	$0m$	$40m/s$	(-1,0)	50%
2.layer	$8000m$	$15m/s$	(1,-1)	25%
3.layer	$12000m$	$30m/s$	(1,0)	25%

Table 1: Characteristics of the turbulent layers of the simulated 3-layers atmosphere. The C_n^2 profile is a measure characterizing the amount of turbulence located on a specific layer.

Proposition 3 suggests that we need at least $K = L + 1$ wavefronts as input in order to reconstruct L layers. Thus we have chosen $K = 4$, i.e. 5 time steps of length $\Delta_T =$

$0.002s$ as input data. The wavefronts φ_k, i.e., the data, are computed by summation of the shifted atmosphere layers at time $(t - k\Delta_T), k = 0, \cdots, K$, on the larger area. The quality of the reconstructed atmosphere will be estimated on $[-21; 21]^2$. Thus we avoid errors at the edges that arise from the periodic boundary conditions of wavefronts and layers. The cut-off index for the Fourier series for all test cases was chosen as $N_0 = 80$, which also resembles the physical fact that the currently available wavefront sensors cannot resolve higher frequencies.

3.3 Reconstruction of a 3-layers atmosphere from exact data

As a proof of concept we only aim at the reconstruction of the 3-layers atmosphere from undisturbed data $\varphi_0, \cdots, \varphi_4$ according to Algorithm 1. Figure 6 displays the reconstructed atmosphere as well as the original atmosphere. A first visual inspection suggests a good reconstruction quality. However, please note that there is an almost constant offset between the two reconstructions. The relative errors between the original

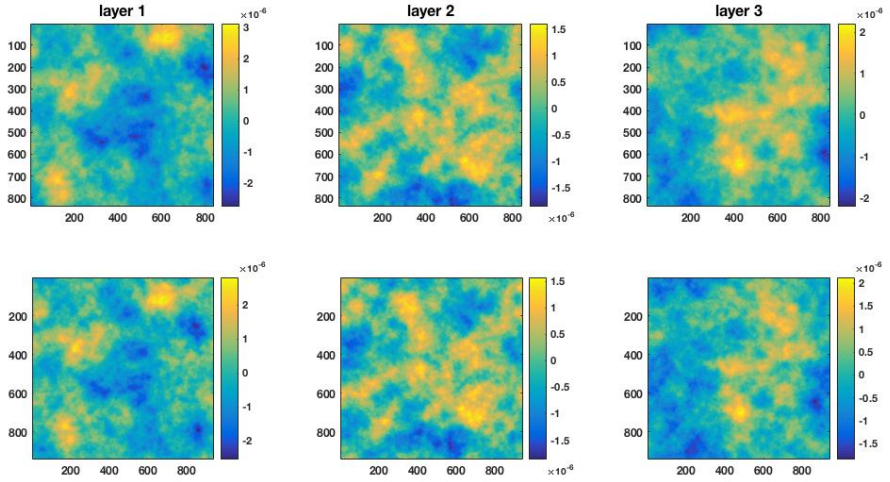

Figure 6: Reconstruction of the 3-layers atmosphere from exact data: The upper row shows the original layer function, the lower row shows the reconstructed layer functions.

layers $\Phi^{(l)}$ and the reconstructed layers $\Phi^{(l)}_{rec}$ on $[-21; 21]^2$ are $(8.8\%, 2.1\%, 12.9\%)$ for $l = 1, 2, 3$, which is large given that we used exact data. Again, the errors are largely due to the offset. A close inspection shows that all the errors are created at indices (j, m) where the matrix A_{jm} is rank deficient: in these cases, the method computes solutions that are perpendicular to $\mathcal{N}(A_{jm})$, a property that is in general not shared by the coefficients from the underlying original atmosphere. Figure 7 displays the coefficients where A_{jm} is (numerically) rank deficient.

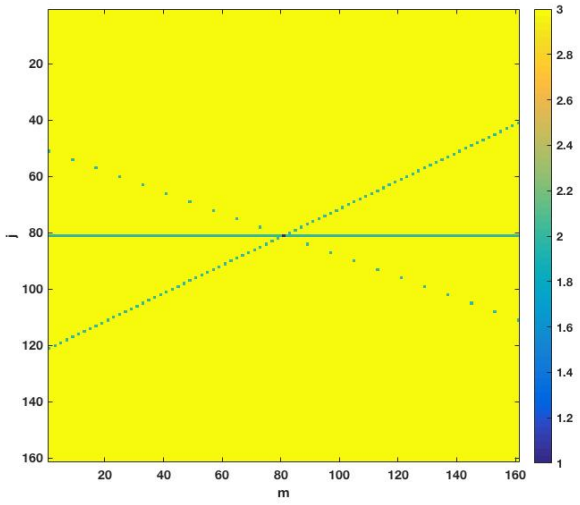

Figure 7: Plot of the rank of the matrices A_{jm} vs indices (j, m). Yellow shows full rank (3), other colors indicate rank deficiencies of the associated matrix.

To verify that the reconstruction of all the coefficients which are related to matrices A_{jm} with full rank is correct we compared the reconstruction quality only on the related set of Fourier coefficients: If we drop all coefficients (j, m) where A_{jm} is rank deficient both in the original and the reconstructed layers, we obtain a perfect reconstruction, see Figure 8. In this case, the relative error between original and reconstructed atmosphere is $\approx 10^{-23}$ and thus within the numerical accuracy. This confirms that our proposed method is able to reconstruct a solution to the atmospheric tomography problem at least on $\mathcal{N}(\boldsymbol{A})^{\perp}$.

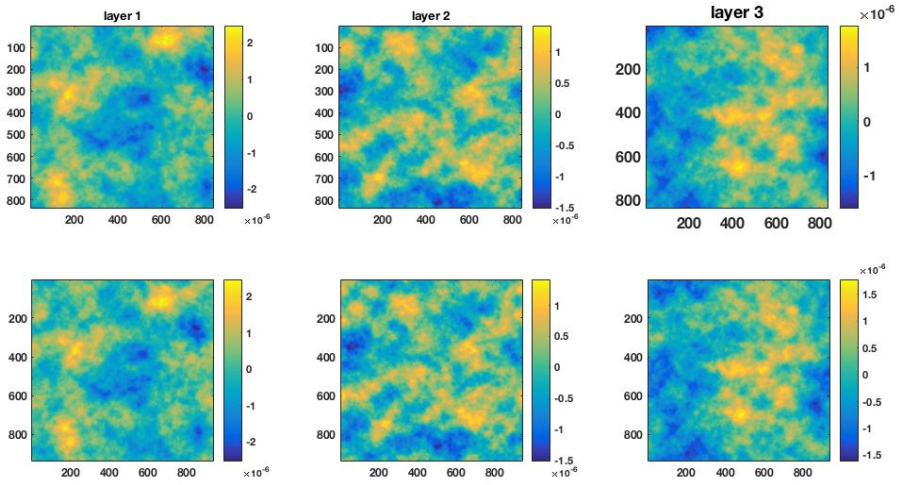

Figure 8: 3-layers atmosphere from exact data restricted to Fourier coefficients for full rank A_{jm}: The upper row shows the restricted original layer function, the lower row shows the restricted reconstructed layer functions.

4 Summary and future work

In the previous sections we have developed and analyzed a method that reconstructs the turbulence in the atmosphere above an earthbound telescope based on measurements of incoming wavefronts at different time steps from a Natural Guide Star. The underlying mathematical problem has been analyzed and a reconstruction method has been developed. In future work, several important questions have to be answered: First, appropriate regularization strategies for the inversion of our tomography operator have to be developed. An option is, e.g., to regularize each subsystem with matrix A_{jm} separately. In a second step, the reconstructions have to be carried out using wavefront sensor measurements instead of wavefronts. Finally, the whole algorithm has to be included into a more realistic simulation environment like OCTOPUS from ESO in order to quantify the gain in imaging quality.

5 Acknowledgments

The work of the authors was partially supported by the Austrian Science Fund (FWF), project F 6805-N36: SFB *Tomography Across the Scales* and by the Austrian Ministry of Research (Hochschulraumstrukturmittel) in the project *Observation oriented Astrophysics in the ELT era*. Both autors would like to thank Roland Wagner and Markus Pöttinger for fruitful discussions.

References

[1] D. R. Andersen, S. S. Eikenberry, M. Fletcher, B. L. William Gardhuose, J.-P. Veran, D. Gavel, R. Clare, R. G. L. Jolissaint, R. Julian, and W. Rambold, *The MOAO system of the IRMOS near-infrared Multi-Object Spectrograph for TMT*, Proceedings of the SPIE, 6269 (2006).

[2] G. Auzinger, *New Reconstruction Approaches in Adaptive Optics for Extremely Large Telescopes*, PhD thesis, Johannes Kepler University Linz, 2017.

[3] M. Davison, *The ill-conditioned nature of the limited angle tomography problem*, SIAM J. Appl. Math., 43 (1983), pp. 428–448.

[4] V. Dhillion, *Adaptive optics*. http://www.vikdhillon.staff.shef.ac.uk/teaching/phy217/telescopes/phy2
03 – 16.

[5] E. Diolaiti, A. Baruffolo, M. Bellazzini, V. Biliotti, G. Bregoli, C. Butler, P. Ciliegi, J.-M. Conan, G. Cosentino, S. D'Odorico, B. Delabre, H. Foppiani, T. Fusco, N. Hubin, M. Lombini, E. Marchetti, S. Meimon, C. Petit, C. Robert, P. Rossettini, L. Schreiber, and R. Tomelleri, *MAORY: A Multi-conjugate Adaptive Optics RelaY for the E-ELT*, Messenger, (2010), pp. 28–9.

[6] B. Ellerbroek, L. Gilles, and C. Vogel, *A computationally efficient wavefront reconstructor for simulation or multi-conjugate adaptive optics on giant telescopes*, Proc. SPIE, 4839 (2002).

[7] B. Ellerbroek and C. Vogel, *Inverse problems in astronomical adaptive optics*, Inverse Problems, 25 (2009), p. 063001.

[8] T. Fusco, J.-M. Conan, G. Rousset, L. Mugnier, and V. Michau, *Optimal wave-front reconstruction strategies for multi conjugate adaptive optics*, J. Opt. Soc. Am. A, 18 (2001), pp. 2527–2538.

[9] L. Gilles and B. Ellerbroek, *Split atmospheric tomography using laser and natural guide stars*, J. Opt. Soc. Am., 25 (2008), pp. 2427–35.

[10] L. Gilles, B. Ellerbroek, and C. Vogel, *Layer-oriented multigrid wavefront reconstruction algorithms for multi-conjugate adaptive optics*, Proc. SPIE, 4839 (2002).

[11] L. Gilles, B. Ellerbroek, and C. Vogel, *Preconditioned conjugate gradient wavefront reconstructors for multiconjugate adaptive optics*, Applied Optics, 42 (2003), pp. 5233–5250.

[12] L. Gilles, B. Ellerbroek, and C. Vogel, *A comparison of Multigrid V-cycle versus Fourier Domain Preconditioning for Laser Guide Star Atmospheric Tomography*, in Adaptive Optics: Analysis and Methods/Computational Optical Sensing and Imaging/Information Photonics/Signal Recovery and Synthesis Topical Meetings on CD-ROM, OSA Technical Digest (CD), Optical Society of America, 2007.

[13] V. L. C. F. Golub, G. H., *Matrix computations*, The Johns Hopkins University Press, Baltimore, 2013.

[14] F. Hammer, F. Sayède, E. Gendron, T. Fusco, D. Burgarella, V. Cayatte, J.-M. Conan, F. Courbin, H. Flores, I. Guinouard, et al., *The FALCON concept: Multi-object spectroscopy combined with MCAO in near-IR*, Scientific Drivers for ESO Future VLT/VLTI Instrumentation ESO Astrophysics Symposia, (2002), pp. 139–148.

[15] T. Helin and M. Yudytskiy, *Wavelet methods in multi-conjugate adaptive optics*, Inverse Problems, 29 (2013), p. 085003.

[16] J. C. R. Horn, R. A., *Topics in matrix analysis*, Cambridge University Press, 1991.

[17] F. Natterer, *The Mathematics of Computerized Tomography*, Wiley, 1986.

[18] A. Neubauer and R. Ramlau, *A singular-value-type decomposition for the atmospheric tomography operator*, SIAM Journal on Applied Mathematics, 77 (2017), pp. 838–853.

[19] M. Pöttinger, R. Ramlau, and G. Auzinger, *A new temporal control approach for SCAO systems*, Inverse Problems, 36 (2019), p. 015002.

[20] M. Puech, H. Flores, M. Lehnert, B. Neichel, T. Fusco, P. Rosati, J.-G. Cuby, and G. Rousset, *Coupling MOAO with integral field spectroscopy: specifications for the VLT and the E-ELT*, Mon. Not. R. Astron. Soc., 390 (2008), pp. 1089–1104.

[21] S. Raffetseder, R. Ramlau, and M. Yudytskiy, *Optimal mirror deformation for multi conjugate adaptive optics systems*, Inverse Problems, 32 (2016), p. 025009.

[22] R. Ramlau, A. Obereder, M. Rosensteiner, and D. Saxenhuber, *Efficient iterative tip/tilt reconstruction for atmospheric tomography*, Inverse Problems in Science and Engineering, 22 (2014), pp. 1345–1366.

[23] R. Ramlau and M. Rosensteiner, *An efficient solution to the atmospheric turbulence tomography problem using Kaczmarz iteration*, Inverse Problems, 28 (2012), p. 095004.

[24] F. Rigaut, B. Ellerbroek, and R. Flicker, *Principles, limitations and performance of multiconjugate adaptive optics*, Proc. SPIE, 4007 (2000), pp. 1022–1031.

[25] C. Robert, J.-M. Conan, D. Gratadour, L. Schreiber, and T. Fusco, *Tomographic wavefront error using multi-LGS constellation sensed with shack-hartmann wavefront sensors*, JOSA A, 27 (2010), pp. A201–A215.

[26] F. Roddier, *Adaptive Optics in Astronomy*, Cambridge, U.K. ; New York : Cambridge University Press, Cambridge, 1999.

[27] M. C. Roggemann and B. Welsh, *Imaging through turbulence*, CRC Press laser and optical science and technology series, CRC Press, 1996.

[28] M. Rosensteiner, *Wavefront reconstruction for extremely large telescopes via CuRe with domain decomposition*, J. Opt. Soc. Am. A, 29 (2012), pp. 2328–2336.

[29] M. Rosensteiner and R. Ramlau, *The Kaczmarz algorithm for multi-conjugate adaptive optics with laser guide stars*, J. Opt. Soc. Am. A, 30 (2013), pp. 1680–1686.

[30] D. Saxenhuber and R. Ramlau, *A gradient-based method for atmospheric tomography*, Inverse Problems and Imaging, 10 (2016), pp. 781–805.

[31] M. Tallon, I. Tallon-Bosc, C. Béchet, F. Momey, M. Fradin, and E. Thiébaut, *Fractal iterative method for fast atmospheric tomography on extremely large telescopes*, in Proc. SPIE 7736, Adaptive Optics Systems II, 2010, pp. 77360X–77360X–10.

[32] E. Thiébaut and M. Tallon, *Fast minimum variance wavefront reconstruction for extremely large telescopes*, J. Opt. Soc. Am. A, 27 (2010), pp. 1046–1059.

[33] Q. Yang, C. Vogel, and B. Ellerbroek, *Fourier domain preconditioned conjugate gradient algorithm for atmospheric tomography*, Applied Optics, 45 (2006), pp. 5281–5293.

[34] M. Yudytskiy, T. Helin, and R. Ramlau, *Finite element-wavelet hybrid algorithm for atmospheric tomography*, J. Opt. Soc. Am. A, 31 (2014), pp. 550–560.

[35] M. Zhariy, A. Neubauer, M. Rosensteiner, and R. Ramlau, *Cumulative wavefront reconstructor for the Shack-Hartman sensor*, Inverse Problems and Imaging, 5 (2011), pp. 893–913.